Chemical Science

ROYAL SOCIETY OF CHEMISTRY

EDGE ARTICLE

View Article Online
View Journal | View Issue

Cite this: *Chem. Sci.*, 2024, **15**, 10027

All publication charges for this article have been paid for by the Royal Society of Chemistry

Received 30th March 2024
Accepted 7th May 2024

DOI: 10.1039/d4sc02102a

rsc.li/chemical-science

Facile synthesis of a hydrazone-based zinc(II) complex for ferroptosis-augmented sonodynamic therapy†

Dan Li,‡[a] Minghui Fan,‡[a] Haobing Wang,‡[a] Yongjie Zhu,[a] Bole Yu,[c] Pingyu Zhang *[a] and Huaiyi Huang *[b]

Sonodynamic therapy (SDT), as a novel non-invasive cancer treatment modality derived from photodynamic therapy (PDT), has drawn much attention due to its unique advantages for the treatment of deep tumors. Zinc-based complexes have shown great clinical prospect in PDT due to their excellent photodynamic activity and biosafety. However, their application in SDT has lagged seriously behind. Exploring efficient zinc-based complexes as sono-sensitizers remains an appealing but significantly challenging task. Herein, we develop a hydrazone ligand-based zinc complex (**ZnAMTC**) for SDT of tumors *in vitro* and *in vivo*. **ZnAMTC** was facilely synthesized *via* a two-step reaction from low-cost raw materials without tedious purification. It shows negligible dark toxicity and can produce singlet oxygen ($^1O_2$) under ultrasound (US) irradiation, exhibiting high sono-cytotoxicity to various cancer cells. Mechanism studies show that **ZnAMTC** can effectively reduce the levels of glutathione (GSH) and glutathione peroxidase 4 (GPX4) under US irradiation and later cause ferroptosis of cancer cells. *In vivo* studies further demonstrate that **ZnAMTC** exhibits efficient tumor growth inhibition under US irradiation and has good biosafety. This work provides useful insights into the design of first-row transition metal complexes for SDT application.

Introduction

The development of photodynamic therapy (PDT) based on light irradiation has been greatly restricted *in vivo* due to the limited tissue penetration of light, which is considered to be the Achilles' heel of PDT.[1–3] Sonodynamic therapy (SDT), a novel non-invasive cancer treatment modality derived from PDT, has drawn much attention in fundamental research and clinical application in recent years.[4–7] In SDT, ultrasound (US) is employed as the excitation source instead of light to activate sono-sensitizers and induce the generation of highly cytotoxic reactive oxygen species (ROSs), leading to damage to the cancer cells.[8–11] The potential mechanism indicated that US irradiation can induce ultrasonic cavitation, which further causes sonoluminescence and pyrolysis to activate sonosensitizers, resulting in the generation of ROSs.[12] By virtue of the deep tissue penetration (>10 cm) ability of US, SDT offers great promise to eradicate deep-seated tumor tissue.[13–15]

The sonodynamic activity and biosafety are two key factors for the clinical applications of sono-sensitizers. Up to now, various inorganic nanomaterials have been widely explored for SDT,[16–21] but their uncertain composition and poor biosafety could hinder their practical applications. Small molecule sonosensitizers have gained wide attention due to their well-defined chemical and physical properties. Some are mainly derived from traditional photosensitizers, such as the organic small molecule chlorin e6 (**Ce6**) and transition metal complex tripyridinium ruthenium ($[Ru(bpy)_3]^{2+}$), which can exhibit photodynamic and sonodynamic activities.[5a,22] Among them, transition metal complexes can exhibit superior photodynamic or sonodynamic performance to organic small molecules due to the heavy atom effect,[23,24] but their potential physiological toxicity limits their further clinical applications.

Compared with expensive heavy metal complexes, most first-row transition metal complexes are low in cost, earth-abundant and have good biosafety.[25–28] Zinc, as an essential trace element for the human body, participates in the formation of various coenzymes, and its metal complexes have shown great prospects for PDT application.[26–28] For example, Gasser *et al.* designed a bis(dipyrrole) zinc(II) complex, which produced singlet oxygen ($^1O_2$) during light exposure, leading to cell death in various single-layer cancer cell lines and 3D multicellular

[a]*College of Chemistry and Environmental Engineering, Shenzhen University, Shenzhen, 518060, China. E-mail: p.zhang6@szu.edu.cn*

[b]*School of Pharmaceutical Science (Shenzhen), Shenzhen Campus of Sun Yat-sen University, No. 66, Gongchang Road, Shenzhen 518107, China*

[c]*Laboratory of Life Science, Shenzhen Research Institute of the Hong Kong Polytechnic University, Shenzhen, 518057, China*

† Electronic supplementary information (ESI) available. See DOI: https://doi.org/10.1039/d4sc02102a

‡ These authors contributed equally.

tumor spheres without showing any dark toxicity.[27] Our group also reported a biosafe photoisomerizable zinc(II) complex that can inhibit microtubule polymerization for photoactive therapy.[28] In addition, two zinc phthalocyanines (CGP55847 and photocyanine) have already been in phase II clinical trials.[25a] However, in stark contrast with the flourishing development of zinc-based complexes in PDT applications, research into their SDT applications lags seriously behind. To date, only a few cases of zinc-based complexes have been reported for SDT application, which are mainly focused on the derivatives of zinc porphyrin and phthalocyanine.[12,29] These complexes generally have large planar π-conjugated structures and require tedious multi-step synthesis and purification, greatly impeding their practical applications. Therefore, the development of zinc-based complexes bearing ligands with a simple structure and facile synthesis for SDT is of high interest.

Hydrazones are a class of organic compounds formed by the condensation of a carbonyl group and hydrazine. Many hydrazone-based compounds have been proved to have important biological activities, such as anti-tumor, anti-viral and anti-inflammatory activities; thus, they have become a hot field in current drug research.[30,31] The molecular structure of hydrazone is flexible, selective and sensitive to metal ions, and its metal complexes show prospects in many fields, such as catalysts, light-emitting probes and molecular sensors.[32] In this work, we report a zinc complex (**ZnAMTC**) based on a hydrazone ligand for SDT (Scheme 1). **ZnAMTC** has negligible dark cytotoxicity and produces singlet oxygen ($^1O_2$) under US irradiation; thus, it shows high sono-cytotoxicity to various cancer cells. Mechanism studies show that **ZnAMTC** can effectively reduce the levels of glutathione (GSH) and glutathione peroxidase 4 (GPX4) under US irradiation and later cause ferroptosis of the cancer cells. *In vivo* studies further demonstrate that **ZnAMTC** can inhibit tumor growth under US irradiation and has good biosafety.

Results and discussion

Synthesis and characterization

Zinc(II) complex **ZnAMTC** was facilely synthesized *via* a two-step reaction from cheap raw materials without tedious purification, with a high overall yield of 76%. The synthesis route of **ZnAMTC** is presented in the Experimental section and Fig. 1a. The

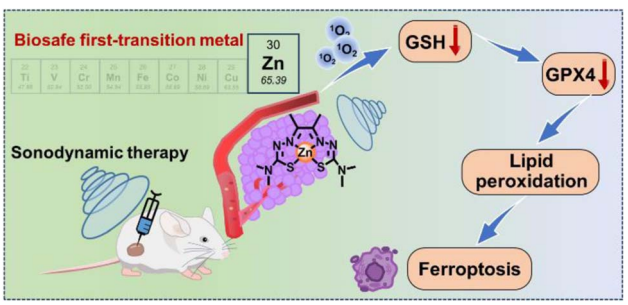

Scheme 1 Schematic illustration of zinc(II) complex for ferroptosis-augmented sonodynamic therapy.

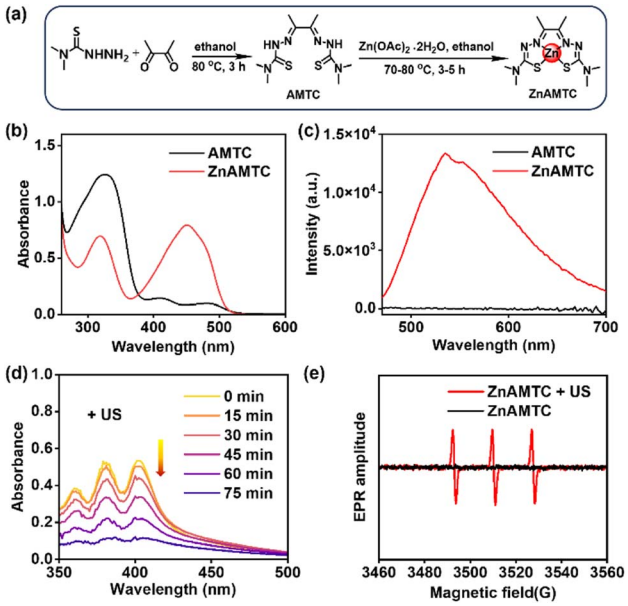

Fig. 1 (a) Synthetic route for **ZnAMTC**. (b) UV-vis absorption and (c) emission spectra of **AMTC** and **ZnAMTC** dispersed in water at 298 K (λ_{ex} = 450 nm). (d) Time-dependent absorption of DPA, suggesting $^1O_2$ generation by **ZnAMTC** under US irradiation. (e) ESR signals of TEMP for characterization of the $^1O_2$ produced by **ZnAMTC** under US irradiation.

hydrazone ligand biacetyl bis(4,4-dimethyl-3-thiosemicarbazone) (**AMTC**) and zinc(II) complex **ZnAMTC** were fully characterized using NMR and ESI-MS spectroscopy (Fig. S1–S4†). The purity of the complex was determined to be 99.8% *via* high performance liquid chromatography (HPLC) analysis (Fig. S5†). As shown in Fig. 1b and c, the maximum absorption wavelength of **AMTC** in a water medium (containing 1% DMSO) was 326 nm. However, the maximum absorption wavelength of **ZnAMTC** was 451 nm, showing an obvious red-shift relative to the ligand, mainly due to the metal-to-ligand charge transfer (MLCT) transition. In addition, **ZnAMTC** showed stronger orange emission than that of the ligand. The emission lifetime of **ZnAMTC** in a water medium (containing 5% DMSO) was 3.5176 ns (Fig. S6†). In addition, after storage in MeOH for 24 h in the dark, the HPLC result of **ZnAMTC** did not change, indicating its good stability in MeOH (Fig. S7†). To investigate the stability of **ZnAMTC** under physiological conditions, the UV-Vis absorption spectra of **ZnAMTC** (10 μM) in a mixture of PBS plus 10% fetal bovine serum (FBS) (containing 5% DMSO) was monitored (Fig. S8†). After storage for 48 h in the dark, the absorption spectra of **ZnAMTC** presented negligible changes, indicating its excellent stability. In addition, we explored the stability of **ZnAMTC** under US irradiation (Fig. S9†). The results showed that the ^1H NMR spectrum of **ZnAMTC** did not change under US irradiation for 20 min, proving its good sono-stability.

ROS generation *via* US irradiation

To explore whether **ZnAMTC** could produce ROS under US irradiation, the probe 9,10-diphenanthraquinone (DPA), which

can be oxidized to DPA dioxide (DPO2) with no characteristic absorption, was first used to detect $^1O_2$.[33] With increasing US irradiation time, the absorption of DPA in the presence of **ZnAMTC** in a water medium (containing 10% DMSO) decreased constantly as it was oxidized to DPO2 (Fig. 1d). However, DPA oxidation by **ZnAMTC** without US irradiation did not occur (Fig. S10†). Subsequently, the probe singlet oxygen sensor green (SOSG) was used to further measure $^1O_2$ in solution.[34] As shown in Fig. S11,† there was no obvious change in the fluorescence intensity of SOSG in the absence of **ZnAMTC**. In contrast, the fluorescence intensity of SOSG increased gradually in the presence of **ZnAMTC** in a water medium (containing 2% DMSO) after US irradiation, indicating the $^1O_2$ generation of **ZnAMTC**.

Then, we detected the generation of different ROS by **ZnAMTC** using electron spin resonance (ESR) spectroscopy. 5,5-Dimethyl-1-pyrroline-*N*-oxide (DMPO) and 2,2,6,6-tetramethylpiperidine (TEMP) were used as spin-trap agents to inspect the generation of $^1O_2$ and hydroxyl radicals (˙OH), respectively. As shown in Fig. 1e, a strong three-line signal was observed between 3460 and 3560 G in **ZnAMTC** and TEMP solution under US irradiation. In contrast, no signal was observed without US irradiation. In ZnAMTC and DMPO solution, the signal of DMPO/˙OH adducts were not observed in either the absence or presence of US irradiation (Fig. S12†). The results showed that **ZnAMTC** could produce $^1O_2$ but not ˙OH after US irradiation.

To study the intracellular ROS generation of **ZnAMTC** for SDT, 2,7-dichlorofluorescein diacetate (DCFH-DA) and SOSG were used to monitor the generation of total ROS and $^1O_2$, respectively. As shown in Fig. S13,† no obvious fluorescence signals were observed in control groups (control, **ZnAMTC** alone and US irradiation alone groups). In contrast, the **ZnAMTC** + US group exhibited evident green fluorescence from DCFH-DA and SOSG oxidation by $^1O_2$, suggesting that **ZnAMTC** can efficiently generate $^1O_2$ in 4T1 cells.

Intracellular localization

The intracellular localization of **ZnAMTC** was monitored by tracking its luminescence using confocal laser scanning microscopy (CLSM). As the incubation time was increased from 2 h to 8 h, it was found that **ZnAMTC** was abundantly internalized into 4T1 cells even after only 2 h incubation (Fig. S14†). To study its subcellular localization accurately, we further used co-staining with commercial lysosome or mitochondrial dyes (Fig. S15†). The results showed that the bright green spots of **ZnAMTC** overlapped with the lysosomal probe (Lyso-Tracker Deep Red, LTDR). The Pearson's colocalization coefficient (PCC) with LTDR had a high value of 0.80. In contrast, almost no overlap could be observed between the luminescence regions of **ZnAMTC** and Mito-Tracker Deep Red (MTDR). The PCC value with MTDR was only 0.19. The results indicated that **ZnAMTC** specifically targeted the lysosomes of 4T1 cells.

Sono-toxicity *in vitro*

Encouraged by the efficient ROS generation of **ZnAMTC** upon US irradiation, we further measured the cytotoxicity of **ZnAMTC** under US irradiation. An experimental diagram of the cells under US irradiation is shown in Fig. S16.† A US irradiation power of 3 W cm^{-2} and an irradiation time of 20 min were selected according to our previous reported work.[5c] The complex was incubated for 4 h, and then, the sono-cytotoxicity of **ZnAMTC** toward various cell lines was evaluated (Table 1 and Fig. 2a and S17†). The IC_{50} value of **ZnAMTC** after 4 h incubation without US irradiation was >100 μM in normal cells (L02) (Fig. S18†). These results suggested that **ZnAMTC** had good biosafety. However, after 20 min of US irradiation, the IC_{50} value of **ZnAMTC** was 2.16 ± 0.05 μM toward 4T1 cells. Other types of the cancer cells were further used to test the sono-cytotoxicity of **ZnAMTC**. The IC_{50} values of **ZnAMTC** toward these cancer cells were all below 20 μM. Additionally, the commonly used sonosensitizer chlorin e6 (**Ce6**) was selected as a control. We evaluated the sono-cytotoxicity of **Ce6** toward 4T1 cells. As shown in Fig. S19,† the IC_{50} of **Ce6** was 33.46 μM. These results indicated that **ZnAMTC** had better cytotoxicity than **Ce6**, suggesting that **ZnAMTC** had great potential for SDT of cancer.

To validate the US-triggered cytotoxicity of **ZnAMTC** intuitively, a calcein acetoxymethyl ester (calcein AM) and propidium iodide (PI) double-staining approach was used to discern live (green) and dead (red) 4T1 cells. As shown in Fig. 2b, a strong green fluorescence signal was observed in the control, **ZnAMTC** alone, and US irradiation alone groups, indicating that the cells remained alive in these control groups. In contrast, an obvious red fluorescence signal was detected upon US irradiation for 20 min in the **ZnAMTC** + US group, illustrating that **ZnAMTC** can kill 4T1 cells efficiently under US irradiation.

Ferroptosis mechanism

It has been reported that the generation of large amounts of ROS can cause ferroptosis in the cancer cells.[35,36] This led us to consider whether the use of **ZnAMTC** for SDT could induce ferroptosis. GSH is closely related to ferroptosis; thus, we first evaluated the ability of **ZnAMTC** to consume GSH. As shown in Fig. 3a and S20,† with increasing US irradiation time, the absorption at 412 nm decreased, indicating that **ZnAMTC**, when irradiated, could consume GSH. We further detected GSH levels in the cells and found that the GSH level in the **ZnAMTC** + US group was significantly lower than that in the other three groups (control, **ZnAMTC** alone, and US alone groups) (Fig. 3b). It can

Table 1 Dark- and sono-cytotoxicity (IC_{50}, μM) of ZnAMTC towards different cancer cells

Cell line	Dark[a] [μM]	US[b] [μM]	SI[c]
HepG2	>100	4.56 ± 0.05	>21.93
A549	>100	11.07 ± 0.03	>9.03
4T1	>100	2.16 ± 0.05	>46.30
HeLa	>100	19.62 ± 0.04	>5.10
L02	>100	N.D.	N.D.

[a] 4 h drug exposure in the dark followed by drug-free incubation for another 44 h in the dark. [b] 4 h drug exposure followed by US irradiation (1.0 MHz, 3 W cm^{-2}, 10% duty cycle) and drug-free incubation for another 44 h in the dark. Data are shown as mean ± SD (n = 6). [c] The sonodynamic index (SI) is defined as IC_{50}, dark/IC_{50}, US. N.D. = not detected.

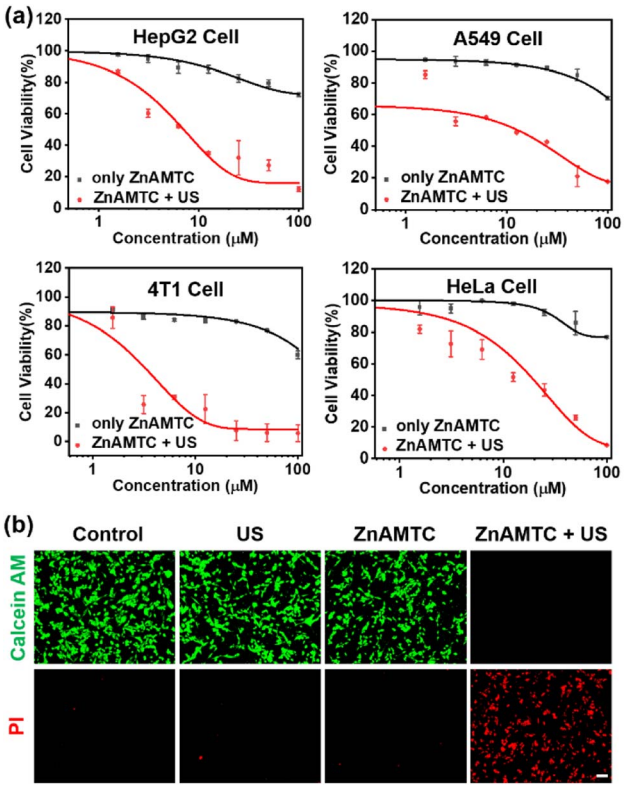

Fig. 2 (a) Cell viability of various cancer cells incubated with different concentrations of **ZnAMTC** in the absence or presence of US irradiation for 20 min. Data are shown as mean ± SD ($n = 6$). (b) Images of 4T1 cells co-stained with calcein AM (4 μM, 0.5 h) and propidium iodide (6 μM, 0.5 h) after different treatments. Scale bar: 100 μm. Calcein AM: λ_{ex} = 460 nm, λ_{em} = 540 ± 30 nm; PI: λ_{ex} = 540 nm, λ_{em} = 610 ± 30 nm. Scale bar: 200 μm. US irradiation: 1.0 MHz, 3 W cm^{-2}, 10% duty cycle, 20 min.

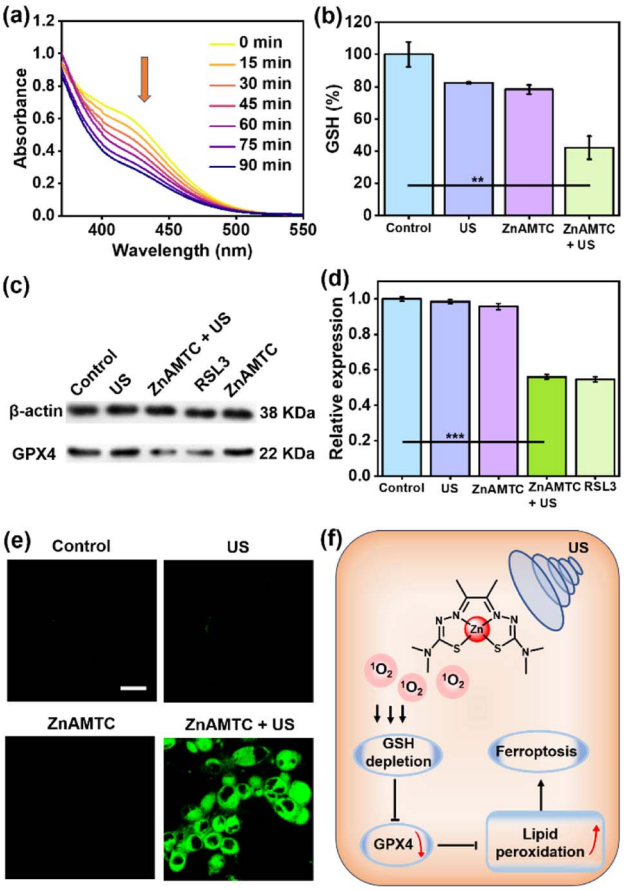

Fig. 3 Ferroptosis induction by **ZnAMTC** under US irradiation. (a) Irradiation-time-dependent GSH (200 μM) depletion by **ZnAMTC** (50 μM) upon US irradiation at 298 K. (b) GSH levels in 4T1 cells after different treatments. Data are shown as mean ± SD ($n = 4$). Statistical significance was calculated using a two-tailed Student's t-test, $^*p < 0.05$, $^{**}p \leq 0.01$ or $^{***}p \leq 0.001$. (c) Western blot analysis of GPX4 in 4T1 cells after different treatments. (d) Relative expression levels of GPX4 calculated from (c). Data are shown as mean ± SD ($n = 4$). Statistical significance was calculated using a two-tailed Student's t-test, $^*p < 0.05$, $^{**}p \leq 0.01$ or $^{***}p \leq 0.001$. (e) Fluorescence images of 4T1 cells stained with C11-BODIPY after different treatments. C11-BODIPY: λ_{ex} = 488 nm; λ_{em} = 570 ± 50 nm; scale bar: 20 μm; US irradiation: 1.0 MHz, 3 W cm^{-2}, 10% duty cycle, 20 min. (f) Mechanism of ferroptosis in the SDT process.

be concluded that **ZnAMTC** can induce the degradation of GSH levels in cells under US irradiation.

Ferroptosis is iron-dependent cell death resulting from excessive lipid peroxidation. The key characteristic of ferroptosis is the peroxidation of phospholipids with polyunsaturated fatty acids on the cell membrane after the cell antioxidant capacity is compromised, leading to membrane damage and ferroptosis. The enzyme glutathione peroxidase 4 (GPX4) plays a crucial role in neutralizing lipid peroxides in a glutathione-dependent manner and inhibiting GPX4 triggers ferroptosis. Depletion of GSH indirectly suppresses GPX4 expression.[37,38] We speculated that **ZnAMTC** could further suppress GPX4 expression, which was confirmed through western blot analysis. The classical ferroptosis inducer RSL3, which can directly inhibit the catalytic activity of GPX4, was used as a positive control.[39] As shown in Fig. 3c and d and S21,† the **ZnAMTC** alone and US irradiation alone groups did not inhibit the expression of GPX4. However, **ZnAMTC** in the presence of US irradiation can significantly reduce GPX4 expression, similar to that of the RLS3-treated group, indicating that **ZnAMTC** can effectively induce ferroptosis under US exposure.

The lipid peroxides in the cancer cells were measured using a C11-BODIPY probe and observed using a laser confocal microscope.[40] **ZnAMTC** was incubated with 4T1 cells for 4 h, exposed to US irradiation for 20 min, and incubated with 50 μM C11-BODIPY. As shown in Fig. 3e, C11-BODIPY emitted bright green fluorescence in the **ZnAMTC** + US group, and the fluorescence intensity was much higher than that in the group exposed to dark conditions. Therefore, the mechanism of tumor cell death caused by **ZnAMTC** was probably ferroptosis. The generation of $^1O_2$ through SDT can effectively consume GSH, inhibit the level of GPX4, causing lipid peroxides and finally inducing ferroptosis (Fig. 3f).

In vivo sonodynamic therapy

We studied the feasibility of **ZnAMTC** for *in vivo* SDT. Since **ZnAMTC** is a small molecule, and there is no specific targeted

group, it can be administered intratumorally. 4T1 tumor-bearing mice were equally divided into four groups (five mice per group): (1) control (PBS solution, 25 μL); (2) US irradiation alone (1.0 MHz, 3 W cm^{-2}, 10% duty cycle); (3) **ZnAMTC** alone (intratumoral injection 25 μL, 500 μM) and (4) **ZnAMTC** + US irradiation (intratumoral injection 25 μL, 500 μM, 1.0 MHz, 3 W cm^{-2}, 10% duty cycle). **ZnAMTC** was injected into the tumor *via* intratumoral injection, followed by US irradiation at day 0 and day 2 post-injections (Fig. 4a). The tumors were then monitored using a digital caliper every 2 days for up to 14 days, and the volumes of the tumors were calculated. As shown in Fig. 4b, the growth of the tumors treated with **ZnAMTC** + US was inhibited compared to the other groups, indicating that **ZnAMTC** effectively suppressed tumor growth after US irradiation. Notably, there was no significant change in body weight in the mice (Fig. S22†), suggesting that the systemic cytotoxicity of **ZnAMTC** was negligible. Finally, all tumor tissues were removed from the mice on day 14 and collected for weighing and photographing. As shown in Fig. 4c and d, the average tumor weight in the **ZnAMTC** + US group was the smallest among all the groups. In addition, hematoxylin and eosin (H&E) staining of 4T1 tumor tissue showed that **ZnAMTC** combined with US irradiation had the highest apoptosis rate and necrotic area, indicating significant damage to tumor cells (Fig. 4e). Interestingly, no significant damage or inflammatory reaction was observed in the major organs of the mice at different days after the injection of **ZnAMTC** (Fig. S23†), indicating that **ZnAMTC** has good biocompatibility and biosafety.

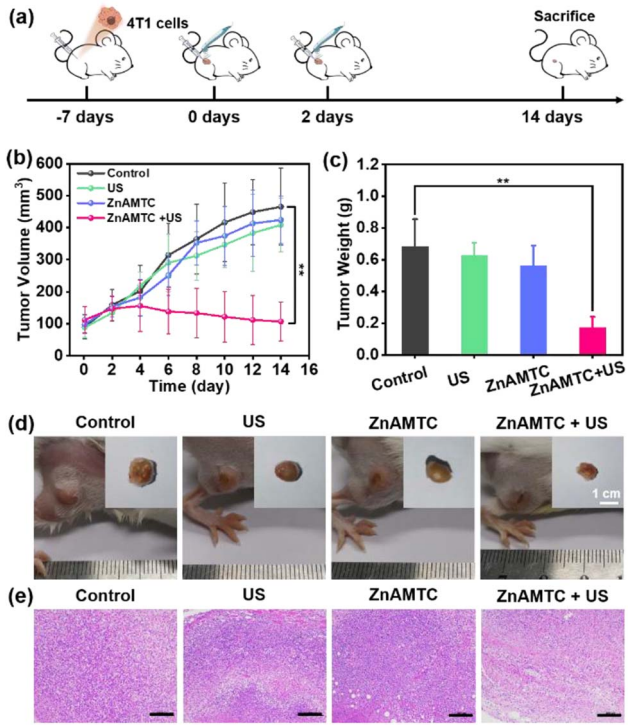

Fig. 4 (a) Schematic of the *in vivo* (4T1 tumor-bearing Balb/c mice) therapeutic protocol. Mice were irradiated by US (1.0 MHz, 3 W cm^{-2}, 10% duty cycle) for 60 min after intratumoral injection with 25 μL of PBS containing 500 μM **ZnAMTC** on day 0 and day 2. (b) Tumor growth curves after treatment. Data are shown as mean ± SD ($n = 5$). Statistical significance was calculated with two-tailed Student's *t*-test, $*p < 0.05$, $**p \leq 0.01$ or $***p \leq 0.001$. (c) Tumor weights of mice at day 14 after various treatments. Data are shown as mean ± SD ($n = 5$). Statistical significance was calculated with two-tailed Student's *t*-test, $*p < 0.05$, $**p \leq 0.01$ or $***p \leq 0.001$. (d) Digital photos of representative mice after various treatments. (e) H&E staining images of tumor slides from mice after different treatments. Scale bars: 200 μm.

Conclusions

In summary, a biosafe zinc(II) complex based on a hydrazone ligand was developed for SDT of tumors. *In vitro* experiments showed that **ZnAMTC** exhibited negligible dark toxicity. Upon US irradiation, it can produce ROSs efficiently and kill various types of cancer cells. Mechanism studies showed that **ZnAMTC** can significantly down-regulate the GSH content in 4T1 cells under US irradiation, resulting in the accumulation of lipid peroxides and ultimately inducing ferroptosis. *In vivo* studies revealed that **ZnAMTC** can effectively inhibit 4T1 tumor growth and did not damage normal cells and tissues. This work provided a new idea for designing biosafe first-row transition metal complexes for efficient SDT.

Experimental section

Materials and instruments

All reagents and solvents were of the highest quality available from commercial sources and were used without further purification. The reagents 4,4-dimethyl-3-thiosemicarbazide, 2,3-butanedione, zinc acetate dihydrate, and concentrated H_2SO_4 were obtained from Aladdin. 3-(4,5-Dimethylthiazol-2-yl)-2,5-diphenyltetrazolium bromide (MTT), 9,10-diphenylanthracene (DPA), 5,5-dimethyl-1-pyrroline *N*-oxide (DMPO), and 2,2,6,6-tetramethylpiperidine (TEMP) were purchased from Sigma-Aldrich. Singlet Oxygen Sensor Green (SOSG), Mitotracker® Deep Red and LysoTracker® Deep Red were obtained from KeyGen BioTECH. 2′,7′-Dichlorofluorescin diacetate (DCFH-DA), GSH and GSSG Assay kit were obtained from Beyotime Biotechnology. C11-BODIPY was purchased from Cayman Chemical. 4T1 breast cancer cell line (4T1), HepG2 human liver hepatocellular carcinoma cell line (HepG2), Henrietta Lacks cell line (HeLa), A549 human lung carcinoma cell line (A549) and L02 human hepatocyte cell line (L02) were purchased from ECACC. Dulbecco's modified eagle medium (DMEM), fetal calf serum (FCS) and Roswell Park Memorial Institute (RPMI) 1640 were purchased from Gibco.

^1H NMR and ^{13}C NMR spectra were recorded using a BrukerAV-500 spectrometer. UV-visible absorption spectra were recorded using a Hitachi UV-2500 spectrophotometer. The emission spectra and fluorescence lifetime were recorded using an Edinburgh FS5 Spectrofluorometer. HPLC spectra were recorded using an Agilent 1260 high performance liquid chromatograph. ESR spectra were recorded using a Bruker Model A300 ESR spectrometer equipped with a Bruker ER 4122 SHQ resonator. The cellular fluorescence images were recorded using a confocal laser scanning microscope (Zeiss LSM 880) and fluorescence microscopy (Olympus XI 51). A DJO-France SAS

2776 sonicator was used to generate ultrasound during the treatment, and medical ultrasonic couplant was used as a transfer medium between the sonicator and samples. Cell viability assays were recorded using a Promega microplate reader. All plotted and calculated statistical analyses were performed using Excel 2019 and Origin 8.5.

Synthesis of AMTC

4,4-Dimethyl-3-thiosemicarbazide (238 mg, 2 mmol) and 2,3-butanedione (86 mg, 1 mmol) were added to 10 mL of ethanol. Two drops of concentrated H_2SO_4 were added to catalyze the reaction, and the mixture was refluxed at 80 °C for 3 h. Subsequently, the reaction mixture was allowed to cool to room temperature (RT) and stored at 4 °C overnight to ensure complete precipitation, and the precipitate was then collected by filtration. The product was washed with ethanol (10 mL) and dried under vacuum to obtain an orange solid (220 mg, 80%).[41] ^{1}H-NMR (500 MHz, $CDCl_3$) δ 8.42 (s, 2H), 3.40 (s, 12H), and 2.08 (s, 6H).

Synthesis of ZnAMTC

Equal mole amounts of zinc acetate dihydrate (1 mmol, 219 mg) and **AMTC** (1 mmol, 288 mg) were dissolved in 10 mL ethanol with constant stirring. The reaction mixture was refluxed at 70–80 °C for 3–5 h. The reaction was cooled to RT, and the precipitate was collected by filtration, washed with ethanol (2 × 10 mL) and diethyl ether (10 mL), and dried *in vacuo* to obtain an orange solid (334 mg, 95%). ^{1}H-NMR (500 MHz, $CDCl_3$) δ 3.18 (s, 12H), and 2.25 (s, 6H). ^{13}C NMR (151 MHz, DMSO-d_6) δ 178.04, 145.34, 39.40, and 14.27. HRMS: calcd for $C_{10}H_{18}N_6S_2Zn$ (m/z) 350.0326, found: (m/z) 351.0577.

Fluorescence lifetime

The fluorescence lifetime spectra were obtained using an Edinburgh Instruments FS5 spectrofluorometer equipped with a 405 nm pulsed diode laser source using 10 mm path length quartz cuvettes with four transparent polished faces; time-correlated single photon counting (TCSPC) was employed. The sample was measured in a water medium (containing 5% DMSO) at a concentration of 10 μM. The analysis was performed using the software Fluoracle (Edinburgh Instruments).

Analysis of $^1O_2$ generation by DPA probe

The absorbance spectra of 20 μM **ZnAMTC** and 10 μg per mL DPA in a water medium (containing 10% DMSO) were measured using a UV-vis spectrophotometer after different US irradiation times (1.0 MHz, 3 W cm^{-2}, 10% duty cycle). The absorbance changes of DPA at 378 nm were recorded to quantify the generation rate of $^1O_2$.

Analysis of $^1O_2$ generation by SOSG probe

The $^1O_2$ production of **ZnAMTC** in a water medium (containing 2% DMSO) under US irradiation was measured using the SOSG probe. SOSG (1 μM in deionized water) was mixed with **ZnAMTC** (20 μM) solution. After different US irradiation time (1.0 MHz, 3 W cm^{-2}, 10% duty cycle), the fluorescence intensity of SOSG was detected.

Electron spin resonance (ESR) assay

ESR measurements were carried out at ambient temperature under US irradiation (1.0 MHz, 3 W cm^{-2}, 10% duty cycle). The samples were contained in a flat-cell (WG812) positioned in a TM110 cavity (ER4103 TM). ESR parameters were: sweep width 8 mT, 1024 points, time constant 10.24 ms and conversion time 20.48 ms, giving a sweep time of 30 s. Field modulation was applied at 100 kHz and 0.05 mT, and the microwave attenuation was 18 dB (~3.2 mW). 2,2,6,6-Tetramethyl-piperidine (TEMP, 20 mM) was used as a spin-trap agent for $^1O_2$ detection, and 5,5-dimethyl-1-pyrroline-*N*-oxide (DMPO, 45 mM) was used as a spin-trap agent for $^{\bullet}$OH detection.

ROS detection in 4T1 cells

SOSG method: The cells were incubated with **ZnAMTC** (10 μM) for 4 h and later irradiated with US (1.0 MHz, 3 W cm^{-2}, 10% duty cycle) for 20 min. Afterwards, the cells were incubated with 2.5 μM Singlet Oxygen Sensor Green (SOSG) for 30 minutes and washed with PBS. The fluorescence images were immediately observed using confocal microscopy (λ_{ex} = 488 nm; λ_{em} = 525 ± 30 nm).

DCFH-DA method: The cells were incubated with **ZnAMTC** (10 μM) for 4 h and irradiated with US (1.0 MHz, 3 W cm^{-2}, 10% duty cycle) for 20 min. Afterwards, the cells were incubated with 10 μM DCFH-DA for 20 minutes and washed with PBS. The fluorescence images were immediately observed using confocal microscopy (λ_{ex} = 458 nm; λ_{em} = 540 ± 30 nm).

Cellular uptake and localization

4T1 cells were incubated with **ZnAMTC** (10 μM) for 2 h, 4 h, or 8 h, respectively, in confocal dishes. CLSM was then used to observe the intracellular distribution of **ZnAMTC** (λ_{ex} = 488 nm, λ_{em} = 535 ± 20 nm). To further analyze the cellular localization of **ZnAMTC**, the cells were pretreated with the commercial lysosomal probe Lyso-Tracker Deep Red (LTDR, 200 nM) or mitochondrial probe Mito-Tracker Deep Red (MTDR, 200 nM) (LTDR or MTDR: λ_{ex} = 633 nm, λ_{em} = 680 ± 40 nm) for 30 min. The working solution was replaced with culture media, and the cells were then imaged using a LSM 880 confocal laser scanning microscope (Zeiss, Germany).

Cytotoxicity *in vitro*

5 × 10^3 cells per well HepG2, A549, 4T1, and HeLa cells were incubated with different concentrations of **ZnAMTC** for 4 h. Subsequently, the culture media was replaced with fresh culture media, which did not contain the complex. 96-well plates were kept in the dark or irradiated by US for 20 min, respectively (1.0 MHz, 3 W cm^{-2}, 10% duty cycle). After irradiation, they were further incubated for 44 h, and then, MTT (25 μL per well, 5 mg mL^{-1}) was used to stain viable cells in the plates for 4 h. The liquid was discarded. DMSO (150 μL per well) was added, and the optical density was measured at 490 nm using a Promega

microplate reader after shaking gently. The wells containing the cells incubated without the complex were set as the control. The cell viability rate (VR) was calculated according to the equation $VR = (A - A_0)/(A_S - A_0) \times 100\%$, where A is the absorbance of the experimental group, A_S is the absorbance of the control group, and A_0 is the absorbance of the blank group (no cells).

Live/dead cell staining assay

The live and dead cell staining assay was conducted using calcein-AM and PI co-staining. 4T1 cells (5×10^3 per well) were seeded in 96-well plates and incubated overnight at 37 °C in a humidified 5% CO_2 atmosphere. The cells were then incubated with or without **ZnAMTC** (10 μM) for 4 h. After that, the cells were treated with or without US irradiation (1.0 MHz, 3 W cm^{-2}, 10% duty cycle). The cells were stained with calcein-AM and PI for the visualization of live cells and dead/late apoptotic cells according to the manufacturer's suggested protocol.

Depletion of GSH in solution

The consumption of GSH was monitored using UV-vis spectroscopy. **ZnAMTC** (50 μM) was mixed with GSH (200 μM) at room temperature. At different irradiation time points, 50 μL of this solution was added to 450 μL PBS, and later 2 μL 5,5′-dithiobis-(2-nitrobenzoic acid) (DTNB) (10 mg mL^{-1}) was added. The absorption spectra of the supernatant were then measured using UV-vis spectroscopy.

Cellular GSH detection

The **ZnAMTC**-induced GSH concentration variation was determined using a GSH and GSSG Assay Kit (Beyotime). 4T1 cells (1×10^7) in a 13 cm culture dish were treated by **ZnAMTC** at a dose of 30 μM in the dark or under US irradiation for 20 min (1.0 MHz, 3 W cm^{-2}, 10% duty cycle). The incubation time was set at 4 h, and drug-free cells were used as the control. Then, the cellular GSH concentrations of the four groups (50 μM only **ZnAMTC** and **ZnAMTC** + US, only US and control groups) were measured according to the manufacturer's suggested protocol.

Intracellular lipid peroxide measurement

4T1 cells were incubated with **ZnAMTC** (30 μM) for 4 h, followed by incubation with C11-BODIPY (50 μM) for 30 min. After that, the cells were washed with PBS and later irradiated with US (1.0 MHz, 3 W cm^{-2}, 10% duty cycle) for 20 min. The green fluorescence was immediately observed using CLSM with an excitation wavelength of 488 nm and emission collection wavelength from 520 nm to 620 nm.

GPX4 analysis

4T1 cells were seeded in 6-well plates at a density of 4×10^5 per well. After 24 h, **ZnAMTC** was added at a dose of 30 μM for 4 h incubation, the cells were irradiated by US (1.0 MHz, 3 W cm^{-2}, 10% duty cycle) for 20 min. The cells that were not subjected to US irradiation were used as a control, and RSL3 (10 μg mL^{-1}) was a positive control. All the cells were collected. The expression of GPX4 in 4T1 cells upon formulation treatment was analyzed using western blotting according to the protocol method. The cell lysates containing identical protein (40 μg) were subjected to standard electrophoresis, followed by antibody incubation at 4 °C. The dilution ratio for the first antibody was 1 : 2000 (β-actin-specific antibody) and 1 : 2500 (GPX4-specific antibody). Regarding the secondary antibody, the dilution ratio was 1 : 5000 for GPX4 and β-actin. Protein bands were developed *via* the ECLTM western blotting detection reagents.

SDT *in vivo*

Female BALB/c mice (6–8 weeks) were used as an animal model in this work and were purchased from Liaoning Changsheng Biotechnology Co. Ltd. Mice were housed in individually ventilated cage (IVC) systems (ambient temperature: 23 ± 3 °C; relative humidity: 40–70%) and exposed to a 12 h light–dark cycle with free access to food and water. The *in vivo* study was conducted in accordance with the Animal Care and Institutional Ethical Guidance in China. The experiment was authorized by the Animal Research Ethics Committee of Shenzhen University (certificate number SYXK 2022-0302).

To examine *in vivo* tumor growth inhibition by **ZnAMTC**, we randomly divided the 4T1 tumor-bearing mice into four groups ($n = 5$ per group): (i) control group with only PBS injection; (ii) US irradiation group (1.0 MHz, 3 W cm^{-2}, 10% duty cycle, 20 minutes); (iii) **ZnAMTC** group (i.v. injection, 25 μL, 500 μM); and (iv) **ZnAMTC** + US irradiation group (i.v. injection and US irradiation). US irradiation was carried out on day 0, and the size of the tumor was recorded every 2 days. Tumor volume = ((tumor length) × (tumor width)^2)/2. Finally, the mice in different groups were sacrificed, and their tumors were collected for photographing and weighing. The tumor slices were used for H&E staining on the next day.

Statistical analysis

All data were obtained from a minimum of three independent experimental replicates and are presented as mean value ± standard deviation (SD). Statistical significance (P values) was determined using two-tailed Student's t-test, $^*p < 0.05$, $^{**}p \leq 0.01$, and $^{***}p \leq 0.001$. n.s. indicates no significant difference.

Data availability

All experimental supporting data and procedures are available in the ESI.†

Author contributions

M. Fan, H. Huang and P. Zhang designed the study. M. Fan and D. Li synthesized the complex and performed the experiments *in vitro*. H. Wang did the experiments *in vivo*. All authors analyzed the data and wrote the paper.

Conflicts of interest

There are no conflicts of interests to declare.

Acknowledgements

We appreciate the financial support of the Science and Technology Foundation of Shenzhen (JCYJ20210324095200002 (P. Z.), JCYJ20220531103405012 (P. Z.), and RCYX20221008092906021 (P. Z.)), Natural Science Foundation of Guangdong Province (2023B1515020060 (P. Z.) and 2021B1515020050 (H. H.)), and National Natural Science Foundation of China (NSFC, 22077085 (P. Z.), 22177078 (H. H.), and 22277153 (H. H.)). We appreciate the Instrumental Analysis Center of Shenzhen University.

Notes and references

1 D. E. J. G. J. Dolmans, D. Fukumura and R. K. Jain, *Nat. Rev. Cancer*, 2003, **3**, 380–387.
2 M. Lan, S. Zhao, W. Liu, C.-S. Lee, W. Zhang and P. Wang, *Adv. Healthcare Mater.*, 2019, **8**, 1900132.
3 L. Li, J. Fu, J. Ye, L. Liu, Z. Sun, H. Wang, S. Tan, M. Zhen, C. Wang and C. Bai, *Adv. Mater.*, 2024, 2310875.
4 G. Liang, T. Sadhukhan, S. Banerjee, D. Tang, H. Zhang, M. Cui, N. Montesdeoca, J. Karges and H. Xiao, *Angew. Chem., Int. Ed.*, 2023, **62**, e202301074.
5 (*a*) C. Liang, J. Xie, S. Luo, C. Huang, Q. Zhang, H. Huang and P. Zhang, *Nat. Commun.*, 2021, **12**, 5001; (*b*) Y. Li, N. Lu, Q. Lin, H. Wang, Z. Liang, Y. Lu and P. Zhang, *Chin. Chem. Lett.*, 2022, **34**, 107653; (*c*) J. Xie, C. Liang, S. Luo, Z. Pan, Y. Lai, J. He, H. Chen, Q. Ren, H. Huang, Q. Zhang and P. Zhang, *ACS Appl. Mater. Interfaces*, 2021, **13**, 27934–27944; (*d*) Y. Lai, N. Lu, A. Ouyang, Q. Zhang and P. Zhang, *Chem. Sci.*, 2022, **13**, 9921; (*e*) Y. Li, H. Wang, Q. Lin, X. Yu, H. Huang and P. Zhang, *Sci. China: Chem.*, 2023, **66**, 2645–2653.
6 G. Liu, Y. Zhang, H. Yao, Z. Deng, S. Chen, Y. Wang, W. Peng, G. Sun, M.-K. Tse, X. Chen, J. Yue, Y.-K. Peng, L. Wang and G. Zhu, *Sci. Adv.*, 2023, **9**, eadg5964.
7 I. Rosenthal, J. Z. Sostaric and P. Riesz, *Ultrason. Sonochem.*, 2004, **11**, 349–363.
8 S. Son, J. H. Kim, X. Wang, C. Zhang, S. A. Yoon, J. Shin, A. Sharma, M. H. Lee, L. Cheng, J. Wu and J. S. Kim, *Chem. Soc. Rev.*, 2020, **49**, 3244–3261.
9 C. You, X. Li, D. Wang, H. Chen, L. Liang, Y. Chen, Y. Zhao and H. Xiang, *Angew. Chem., Int. Ed.*, 2022, **61**, e202210174.
10 Y. Duan, Y. Yu, P. Liu, Y. Gao, X. Dai, L. Zhang, L. Chen and Y. Chen, *Angew. Chem., Int. Ed.*, 2023, **62**, e202302146.
11 S. Liu, K. Dou, B. Liu, M. Pang, P. Ma and J. Lin, *Angew. Chem., Int. Ed.*, 2023, **62**, e202301831.
12 P. Zhao, Y. Wu, X. Li, L. Feng, L. Zhang, B. Zheng, M. Ke and J. Huang, *Angew. Chem., Int. Ed.*, 2022, **61**, e202113506.
13 (*a*) M. Zhan, F. Wang, Y. Liu, J. Zhou, W. Zhao, L. Lu, J. Li and X. He, *Adv. Sci.*, 2023, **10**, 2207200; (*b*) F. Wang, Y. Fan, Y. Liu, X. Lou, L. Sutrisno, S. Peng and J. Li, *Exploration*, 2024, 20230100.
14 J. Li, Y. Luo, Z. Zeng, D. Cui, J. Huang, C. Xu, L. Li, K. Pu and R. Zhang, *Nat. Commun.*, 2022, **13**, 4032.
15 S. Son, J. H. Kim, X. Wang, C. Zhang, S. A. Yoon, J. Shin, A. Sharma, M. H. Lee, L. Cheng, J. Wu and J. S. Kim, *Chem. Soc. Rev.*, 2020, **49**, 3244–3261.
16 Q. T. Hoang, T. G. N. Cao, S. J. Kang, M. Lee, J. H. Kang, H. S. Park, J.-E. Kim, S. H. Bhang, Y. T. Ko, W. J. Rhee and M. S. Shim, *Chem. Eng. J.*, 2023, **472**, 144871.
17 F. Gong, L. Cheng, N. Yang, Y. Gong, Y. Ni, S. Bai, X. Wang, M. Chen, Q. Chen and Z. Liu, *Nat. Commun.*, 2020, **11**, 3712.
18 C. Li, X. Yang, J. An, K. Cheng, X. Hou, X. Zhang, Y. Hu, B. Liu and Y. Zhao, *Theranostics*, 2020, **10**, 867.
19 Z. Chen, L. Chen, Y. Ma, Y. Liu, Q. Zhang, H. Qin, Y. Chen, B. Tian and J. Dong, *Adv. Mater.*, 2023, **35**, 2304246.
20 D. Wen, K. Li, R. Deng, J. Feng and H. Zhang, *J. Am. Chem. Soc.*, 2023, **145**, 3952–3960.
21 G. Feng, H. Huang, M. Zhang, Z. Wu, D. Sun, Q. Chen, D. Yang, Y. Zheng, Y. Chen and X. Jing, *Adv. Sci.*, 2023, **10**, 2302579.
22 D. Li, Y. Yang, D. Li, J. Pan, C. Chu and G. Liu, *Small*, 2021, **17**, 2101976.
23 Y. Xu, Y. Pang, L. Luo, A. Sharma, J. Yang, C. Li, S. Liu, J. Zhan and Y. Sun, *Angew. Chem., Int. Ed.*, 2024, **63**, e202319966.
24 A. K. Yadav, N. Kumar, A. T. Khan, R. Kushwaha and S. Banerjee, *ChemMedChem*, 2022, **17**, e202100615.
25 (*a*) L. Gourdon, K. Cariou and G. Gasser, *Chem. Soc. Rev.*, 2022, **51**, 1167–1195; (*b*) X. Peng, H. Zhang, R. Zhang, Z. Li, Z. Yang, J. Zhang, S. Gao and J. Zhang, *Angew. Chem., Int. Ed.*, 2023, **62**, e202307838; (*c*) J. Shao, J. Xue, Y. Dai, H. Liu, N. Chen, L. Jia and J. Huang, *Eur. J. Cancer*, 2012, **48**, 2086–2096; (*d*) D. Chen, M. Song, J. Huang, N. Chen, J. Xue and M. Huang, *J. Innovative Opt. Health Sci.*, 2020, **13**, 2030009.
26 (*a*) Y. Li, C. Wang, L. Zhou and S. Wei, *Chem. Commun.*, 2021, **57**, 3127–3130; (*b*) M. Zhu, H. Zhang, G. Ran, Y. Yao, Z. Yang, Y. Ning, Y. Yu, R. Zhang, X. Peng, J. Wu, Z. Jiang, W. Zhang, B. Wang, S. Gao and J. Zhang, *Angew. Chem., Int. Ed.*, 2022, **61**, e202204330; (*c*) G. T. Nash, T. Luo, G. Lan, K. Ni, M. Kaufmann and W. Lin, *J. Am. Chem. Soc.*, 2021, **143**, 2194–2199; (*d*) Y. Wang, W. Qiao, Z. Zhao, Z. Zhao and M. Li, *Interdisciplinary Medicine*, 2023, vol. 1, p. e20230010.
27 J. Karges, U. Basu, O. Blacque, H. Chao and G. Gasser, *Angew. Chem., Int. Ed.*, 2019, **58**, 14334–14340.
28 F. Cao, H. Wang, N. Lu, P. Zhang and H. Huang, *Angew. Chem., Int. Ed.*, 2023, **62**, e202301344.
29 A. Ma, H. Chen, Y. Cui, Z. Luo, R. Liang, Z. Wu, Z. Chen, T. Yin, J. Ni, M. Zheng and L. Cai, *Small*, 2019, **15**, 1804028.
30 J. Wahbeh and S. Milkowski, *SLAS Technol.*, 2019, **24**, 161–168.
31 Y. Wang, S. Guo, L. Yu, W. Zhang, Z. Wang, Y. R. Chi and J. Wu, *Chin. Chem. Lett.*, 2024, **35**, 108207.
32 T. Gebretsadik, Q. Yang, J. Wu and J. Tang, *Coord. Chem. Rev.*, 2021, **431**, 213666.
33 K. Lu, P.-Y. Lin, E.-Y. Chuang, C.-M. Shih, T.-M. Cheng, T.-Y. Lin, H.-W. Sung and F.-L. Mi, *ACS Appl. Mater. Interfaces*, 2017, **9**, 5158–5172.
34 N. Lu, Z. Deng, J. Gao, C. Liang, H. Xia and P. Zhang, *Nat. Commun.*, 2022, **13**, 2245.
35 C. Xue, M. Li, C. Liu, Y. Li, Y. Fei, Y. Hu, K. Cai, Y. Zhao and Z. Luo, *Angew. Chem., Int. Ed.*, 2021, **60**, 8938–8947.

36 X. Ding, Z. Wang, Q. Yu, N. Michał, S. Roman, Y. Liu and N. Peng, *Adv. Healthcare Mater.*, 2023, **12**, 2301824.
37 S. J. Dixon and B. R. Stockwell, *Nat. Chem. Biol.*, 2014, **10**, 9–17.
38 H. Liu, S. L. Schreiber and B. R. Stockwell, *Biochemistry*, 2018, **57**, 2059–2060.
39 B. R. Stockwell, J. P. F. Angeli, H. Bayir, A. I. Bush, M. Conrad, S. J. Dixon, S. Fulda, S. Gascón, S. K. Hatzios, V. E. Kagan, K. Noel, X. Jiang, A. Linkermann, M. E. Murphy, M. Overholtzer, A. Oyagi, G. C. Pagnussat, J. Park, Q. Ran, C. S. Rosenfeld, K. Salnikow, D. Tang, F. M. Torti, S. V. Torti, S. Toyokuni, K. A. Woerpel and D. D. Zhang, *Cell*, 2017, **171**, 273–285.
40 H. Yuan, Z. Han, Y. Chen, F. Qi, H. Fang, Z. Guo, S. Zhang and W. He, *Angew. Chem., Int. Ed.*, 2021, **60**, 8174–8181.
41 R. Anjum, D. Palanimuthu, D. S. Kalinowski, W. Lewis, K. C. Park, Z. Kovacevic, I. U. Khan and D. R. Richardson, *Inorg. Chem.*, 2019, **58**, 13709–13723.